Numerical Analysis on Frictional Heat Effect in Polyether-Ether-Ketone (PEEK)/Steel Pair by using OpenFOAM Model

Mohd Zaki Bahrom[1,2], Bukhari Manshoor[1,*], Norfazillah Talib[1], Izzuddin zaman[1], Djamal Hissein Didane[1], Reazul Haq Abdul Haq[1], Mohammad Fahmi Abdul Ghafir[1], Noor Azammi Abdul Murat[2], Zulkifli Mohamed[3], Mohd Nizam Ibrahim[4]

1   Faculty of Mechanical and Manufacturing Engineering, Universiti Tun Hussein Onn Malaysia, Batu Pahat, Johor, Malaysia
2   Universiti Kuala Lumpur Malaysia France Institute, Bandar Baru Bangi, Selangor, Malaysia
3   College of Engineering, Universiti Teknologi MARA, Shah Alam Selangor, Malaysia
4   Maxpirations (M) Sdn Bhd, Sura Gate Commercial Centre, Dungun, Terengganu, Malaysia

ARTICLE INFO	ABSTRACT
	The PEEK material has been applied to a sliding bearing system in a power plant system because of its high mechanical durability. In the solid friction of the PEEK materials, the frictional heat becomes the important factor because the temperature increase due to the frictional heat causes the rapid increase of the frictional coefficient of the specimen. To maintain the low frictional coefficient of the PEEK materials, an effective cooling method for the PEEK materials needs to be developed. In this study, the passive cooling method, which attaches the heat sink to the PEEK materials, was suggested. For evaluating the suggested cooling method of the PEEK materials, the calculation model adopting OpenFOAM, which is open-source software, has been developed. Adopting some functions and libraries of OpenFOAM, the frictional heat, heat resistance, and heat transfer coefficient on the heat sink were modelled. The sliding bearing experiment was conducted and time variation of the temperature and friction coefficient in the ring specimen were measured. The temperature variation in the ring specimen was compared with the calculation result. From the numerical calculation results, the developed calculation model could simulate the temperature-time variation of the ring obtained in the experiment, when the variation of the frictional coefficient, heat resistance, and heat transfer coefficient was modelled appropriately.
	Based on the friction and wear test results, by applying a heat dissipation mechanism to the ring test piece, the calorific value of the PEEK material can be reduced, and it is stable. It was suggested that the friction was maintained.

1. Introduction

Polyether-ether-ketone (PEEK) is a super engineering plastic. It is one of the heat-resistant polymer resins, and the continuous usable temperature is about 240 to 260°C, while the glass transition temperature and melting point are 143°C and 343°C respectively [1]. The heat-resistant

temperature of general-purpose engineering plastics is nearly around 100 to 150°C [2-5]. Hence, the heat resistance of PEEK material is high. The characteristics of PEEK material have an advantage due to its heat resistance and chemical resistance. It also has excellent mechanical properties such as bearings and rolling bearing cages [6]. Until now, engineering plastics have been resistant due to their low thermal properties and low strength while metals have been mainly used for mechanical elements used under harsh conditions and high temperatures. However, in recent years, high-speed slippage has occurred due to the development of PEEK composite materials reinforced by filling with PEEK and carbon fibre [3,4]. Furthermore, PEEK indicates that higher molecular weight is associated with improved resistance against the scratch onset of cracking/material removal and abrasive wear volume loss [7]. It has become possible to use it under harsh conditions such as under high temperatures. Currently, PEEK composite materials are used for water turbine generators, final bearings, rolling bearing cages, oil seal rings, etc [5]. By adding PEEK fibres on the mechanical, the surface analysis results demonstrated more oxidation groups, higher polar surface energy and greater wettability of the PEEK surface due to the UV-irradiation. This considerably improved the PEEK/epoxy adhesion and subsequently [8].

Several researchers have been involved in the evaluation of friction and wear properties of PEEK and PEEK composites under unlubricated and oil-lubricated conditions [9, 10]. Currently, the development of nanocomposite for viability in extreme (vacuum, hydrogen and cryogenic) environments is being investigated [11]. They researched terms of the condition of the glass transition temperature with a friction surface temperature of PEEK under high-speed, oil-lubricated conditions. From their results, they found that when the temperature exceeds 143°C, PEEK softens and a large-scale plastic flow is generated, resulting in a rapid increase in the coefficient of friction and a transition to seizure. The lubrication state of PEEK under oil lubrication changes depending on the friction surface temperature, from fluid lubrication to mixed lubrication, and then seizure. The seizure resistance of PEEK composites filled with raw fibres is further improved compared to pure PEEK [12-16]. Friction surface temperature increases even under non-lubricated conditions. If it continues, the coefficient of friction tends to increase [17, 18].

As mentioned above, the friction and wear characteristics of PEEK materials are very sensitive to the friction surface temperature regardless of whether they are non-lubricated or oil-lubricated. Therefore, to maintain low friction and wear of the PEEK material, the heat resistance performance of the PEEK material itself needs to be further improved. Another method that can be used is to keep the friction surface temperature of the system using PEEK material at a low temperature below the glass transition temperature. Akagaki [17] used the low-temperature air jet cooling method under unlubricated conditions. It is possible to cool the ring test piece and suppress the increase in the friction surface temperature, and as a result, suppress the increase in the friction coefficient.

As a cooling method to reduce frictional heat, seizure prevention is used by using a heat dissipation mechanism from a ring with fins attached. By using this method, a heat sink is attached to the rotating shaft and a PEEK tree that utilizes forced convection heat transfer from the heat sink during rotation. This method uses the energy required for heat dissipation from the rotational energy of the shaft, and its mechanism. This system is a passive and easily practical cooling system. Although the importance of attaching a heat sink to the body has been experimentally suggested [18], only a few reports have been made, and a practical cooling means by installing a heat sink on a rotating body has not been established. To develop a practical cooling method by adding a heat sink to such a rotating body, it is necessary to understand the mechanism and design a heat-dissipating fin with high heat transfer.

For that purpose, numerical analysis of the forced convection heat transfer mechanism of the heat radiation fins around the rotating body, and the heat conduction effect on the ring and heat sink

from the friction surface need to be understood clearly. Previous studies on heat transfer analysis of rotating bodies in friction and wear environments have been conducted under the conditions of lubricating oil dripping. Most of the analysis was conducted [19,20], and there are few research cases in which the frictional heat effect under non-lubricated conditions was evaluated in detail analytically [20,21]. In conventional research, heat transfer between the rotating body and the surrounding fluid is only a simple model. Since the proposed cooling method is a practical system, it is desirable to simulate it by using a commercial software package. However, when considering a practical case for fluid simulation in a rotating body, large-scale parallel computing may be indispensable because it must be performed under high-speed conditions. Therefore, many licenses during parallel calculation cost a lot of money to simulate a phenomenon in a practical environment using a commercial software package that requires a lot of nodes. It is considered essential, and it is difficult to understand the heat transfer mechanism in a rotating body in a real environment. So, in this study, an open-source software simulation capability for large-scale parallel computing, OpenFOAM was used for the simulation work.

Although OpenFOAM is a free license, it has many calculation libraries. The above-mentioned fluid simulation of the rotating body and heat conduction analysis in the composite material is easy, and this software is used. It is considered possible to understand the heat transfer mechanism inside the rotating body. As mentioned, OpenFOAM is capable of a practical phenomenon. While it has the potential to be reproduced, the calculation examples of practical phenomena were done by using another commercial software package. The calculation example by OpenFOAM regarding the heat transfer mechanism in a rotating body is very little compared to a commercial software package especially considering the friction surface. Therefore, the purpose of this study is to construct an analytical model of the heat transfer mechanism of a rotating body during friction using OpenFOAM. The usefulness of this cooling method will be evaluated by comparing a temperature measurement from experiment work [22, 23] of the sliding rotation shaft when the heat sink is attached. Moreover, a comparison also will be made in the rotating body when the heat sink is attached, and the fluid simulation of the rotating body is constructed by constructing the analysis modelling by OpenFOAM.

2. Methodology
2.1 Numerical Method and Model Analysis

Figure 1 shows a schematic diagram of the block-on-ring type friction used for the simulation in this study. The simulation was conducted using the three patterns of ring test as shown in Figure 2. The ring test piece has a diameter of 130 mm and a thickness of 20 mm. Bolts were attached to the surface of the test piece. In this study, there are three types of models were simulated which are the ring without a copper plate (Type A), the ring attached with a copper plate (Type B) and the ring with copper and fin (Type C). The heat transfer mechanism of the rotating body targeted in this research was the heat dissipation from the rotating body to the surroundings due to rotational motion and frictional wear. Both effects of heating the ring will be considered. To consider both effects around the rotating body, it is necessary to couple the fluid analysis and the heat conduction analysis inside the rotating body. To simply evaluate this problem, both simultaneous coupling method that calculates the above with the same analysis mesh is considered as a solution. However, the temperature measurement of the experiment by previous research [6] that was used as a benchmark was fixed to 60 minutes, which is a long time. Therefore, the simultaneous coupling method of fluid and heat conduction analysis requires fluid analysis with a high computational load.
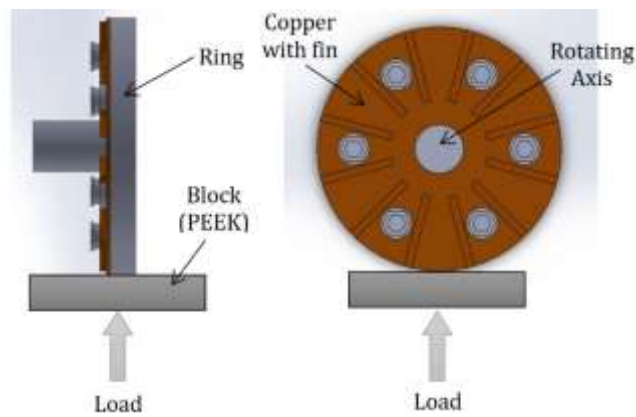
Fig. 1. Schematic diagram of the block-on-ring type friction for the simulation (side and front view)
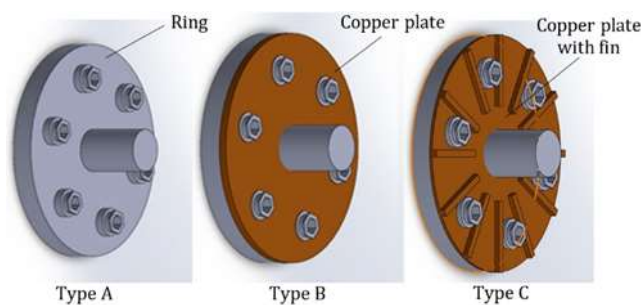
Fig. 2. Rotating ring used for simulation

To solve the above-mentioned problems, the heat transfer mechanism of the rotating body was evaluated by analyzing the heat conduction of the rotating body consisting of the rotating shaft. To understand the heat transfer coefficient, the fluid around the rotating body was analyzed and the amount of convective heat transfer to the ambient air was calculated. The average value of the flow heat transfer amount was set as the boundary condition for the composite heat transfer analysis, and the time change of the temperature of the composite material during friction was obtained. In the calculation process, the wall surface of the rotating body is set to a constant temperature when calculating the convective heat transfer coefficient. For each rotation to be analyzed under actual conditions, the temperature of the rotating body may change depending on the structure of the body. However, this system is forced convection heat transfer by rotational motion.

Therefore, it is assumed that the heat transfer coefficient changes only by the Reynolds number, that is, the rotation speed. Using this assumption, the wall of the fluid analysis was performed with a constant temperature, and the amount of heat transfer was calculated. In the combined heat transfer analysis, the averaged convection heat transfer amount is calculated as metal. It was given as a solid wall boundary condition. In an actual system, the amount of convective heat transfer may change on each wall surface. However, in the system for this study, the biot number, Bi is assumed to be small because it is heat conduction in metal and it is assumed to be a centralized heat capacity model. The analysis method constructed in this study is based on the above assumptions which are the heat transfer coefficient depends only on the Reynolds number and the collection of each component. By using the application of the medium heat capacity model, fluid and heat conduction analysis can be performed independently, and the rotating body can be analyzed. The internal temperature change can be acquired in a short time. In this study, OpenFOAM-v2016 was used in each analysis. The model was constructed, and each analysis method is described below.

2.2 Fluid Analysis Around a Rotating Body

For the numerical fluid analysis around the rotating body, the rotational motion was taken into consideration. In this research, the rotational motion of a rotating body is considered three-dimensionally. Support the energy equation for pimpleDyMFOAM, in which the moving mesh was considered in calculating the considered heat transfer amount. Navier-Stokes equation, which is the governing equation used in this analysis. The energy equation is described by Eq. (1) and (2), respectively.

$$\frac{\partial \bar{u}_i}{\partial t} + \bar{u}_j \frac{\partial \bar{u}_i}{\partial x_j} = \frac{\partial \bar{p}}{\partial x_i} + (v + v_i) \frac{\partial}{\partial x_j} \frac{\partial \bar{u}_i}{\partial x_j} \qquad (1)$$

$$\frac{\partial \bar{T}}{\partial t} + \bar{u}_j \frac{\partial \bar{T}}{\partial x_j} = \left(\alpha + \frac{v_t}{Pr_t} \right) \frac{\partial}{\partial x_j} \frac{\partial \bar{T}}{\partial x_j} \qquad (2)$$

The working fluid is assumed to be an incompressible fluid, and the Navier-Stokes equation with an incompressible approximation shown in Eq. (1) is used. Parameters in the Navier-Stokes equation, u [m/s] is velocity, t [s] is time, x [m] is distance, and p [m^2/s^2] is the corrected pressure, which is the pressure divided by the reference density. v [m^2/s] is the kinematic viscosity coefficient, v_t [m^2/s] indicates the vortex viscosity coefficient. The vortex viscosity coefficient will be described later, but it is modelled by the Reynolds average model. In Eq. (2), T [K] in the energy equation is temperature, α [m^2/s] is the thermal diffusivity, Pr_t is the turbulent Prandtl number. The overbars of the variables in each equation indicate the Reynolds average processing. A simple external flow model of a rotating body using the standard OpenFOAM meshes, blockMesh and snappyHexMesh was produced. The number of grids in the model is around 800,000. Figure 3 shows a cross-sectional view of the mesh of the external flow model. The patch on the surface of the rotating region in Figure 3 is designated as an arbitrary mesh interface (AMI).

The air temperature of 20°C was used as the physical property value of the fluid used in this analysis. As a boundary condition, the velocity gradient was set at the outer wall of the mesh. The pressure gradient was zero (the pressure was zero only on the outlet surface), and the temperature gradient also was set to zero. In addition, the surface of the rotating body should be on the moving surface. A uniform isothermal condition was given on the surface at 100°C with no pressure gradient. The turbulent model used is Reynolds's average with the k-ε model. The turbulent heat flux was modelled with a constant turbulent Prandtl number of 0.7.
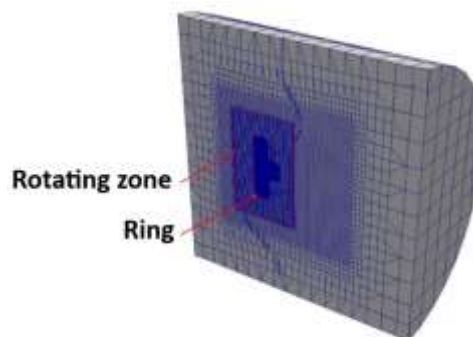
Fig. 3. Cross-section of calculation mesh for simulation work

The differential term was discretized using the complete implicit method, and the time progress was performed. Time progress so that the maximum number of Courant is 0.2 or less was set. The convection term and the diffusion term are the quadratic precision upwind difference method (Gauss linear Upwind grad) and the non-straight mesh. Discretized using the Gauss linear limited corrected 0.33 method with limited second-order accuracy. Then, under each condition of Type A, B, and C, the average heat transfer coefficient of each of the shaft, ring and copper plate parts was calculated. All the parameters and boundary condition settings are summarized in Table 1.

Table 1
Summary of parameters and boundary conditions setting

Sample	Microhardness HV0.05 of the surface material	Microhardness HV0.05 of the material under the surface
C120	349	349
Rp3	438	438

2.3 Thermal Conduction Analysis in a Rotating Body

Thermal conduction analysis in composite materials was performed using chtMultiRegionFoam. The governing equation used in the analysis is shown below,

$$\rho c \frac{\partial T}{\partial t} = k \frac{\partial}{\partial x_j} \frac{\partial T}{\partial x_j} \tag{3}$$

where, ρ [kg/m^3] is the density, c [J/(kg.K)] is the specific heat, and k [W/(m.K)] is the thermal conductivity. The analysis mesh is similar to fluid analysis. It was generated using blockMesh and snappyHexMesh. The number of grids in the analysis mesh is around 100,000 under each condition. Figure 4 shows the analysis model of the derivative analysis using Type C as an example. In this study, the frictional heat is evenly distributed to the ring test piece with a sliding width of 10 mm. When using this assumption, the amount of work per unit time due to frictional heat, W [W] is by the following equation.

$$\dot{W} = \mu P_n V \tag{4}$$

Here, V [m/s] indicates the slip speed of the ring test piece. The amount of work per unit of time is equal to the entire circumference of the ring test piece. Assuming that it affects heat flux, the acting heat flux q [W/m^2] is expressed by the following equation,

$$q = \dot{W}/A \tag{5}$$

where A [m^2] is the product of the sliding width of 10 mm and the circumference of the ring test piece. The friction generated in Figure 4 is shown on the surface. The time derivative term is completely implicit, and the time progress was performed by discretizing using the method. The diffusion term is a quadratic precision centre difference method (Gauss) that corrects the non-orthogonality of the mesh (it was discretized using linear corrected). In the analysis, the analysis mesh of the ring, shaft, and copper plate is used for each constituent material. The shaft end connected to the motor was given adiabatic conditions. The spatial average heat transfer coefficient derived in the analysis was used as the third-class boundary condition.
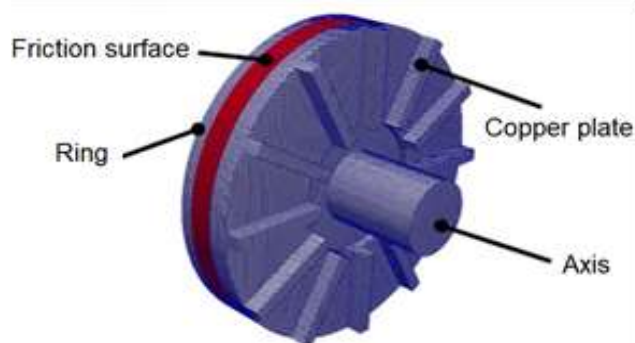
Fig. 4. Mesh for heat conduction simulation for type C

Type 3 boundary conditions of chtMultiRegionFoam were also used for the application. For this type of boundary condition, the ring part and the copper plate are mechanically joined using screws. Therefore, the thermal resistance at the joint is also taken into consideration. In this simulation, chtMultiRegionFoam can add the effect of thermal resistance between arbitrary objects. Besides that, a layer with the maximum height roughness R_z thickness of the copper plate and the ring test piece is generated between the ring test piece and the copper plate. However, the thermal resistance was expressed by giving the thermal conductivity of air. The average value of the maximum height roughness of the copper plate is 1 μm, which is the maximum of the ring test piece. The average value of the height roughness is 5.6 μm. From the above conditions, when the coefficient of friction is taken into consideration, the coefficient of friction and thermal resistance are also taken into consideration.

3. Results
3.1 Air Flow Field around the Rotating Body

Figure 5 shows the visualization result of the velocity distribution around the rotating body 3 seconds after the start of the rotation. For the visualization, the plane including the axis of rotation was the cross section. The maximum wind speed generated by rotation is 1.95 m/s for Type A, 1.94 m/s for Type B and 3.24 m/s for Type C. It was confirmed that the highest flow velocity was generated around the surface of the fins of Type C. In the heat conduction analysis, uniform heat transfer coefficient to the wall surface of each component of the ring, shaft, and copper plate, is regarded as a centralized heat capacity model. However, from this visualization result, the fin surface, that is, copper, is reproduced.

Figure 6 shows the visualization result of the temperature distribution around the ring test piece 3 seconds after the start of the rotation. The results show that it has a uniform temperature distribution of 373 K around the ring tested. The surrounding temperature boundary layer is thicker for Type B compared to the Type A and Type C test pieces. From the shape of the Type B test piece, it is possible that air stagnation occurs on the surface and heat is not dissipated well. The distribution of the temperature also shows that Type B was maintained at a lower temperature compared to Type A. This is due to the heat sink with a high heat conduction effect being added. Due to the more efficient heat exchange, even Type B, which has a low convection effect, is higher than Type A when considering the system. It is considered that the heat dissipation performance was excellent. This result also suggests the importance of adding a heat sink. For the fin effect in Type C, the temperature boundary layer becomes thinner due to the agitation of the fluid around the ring.
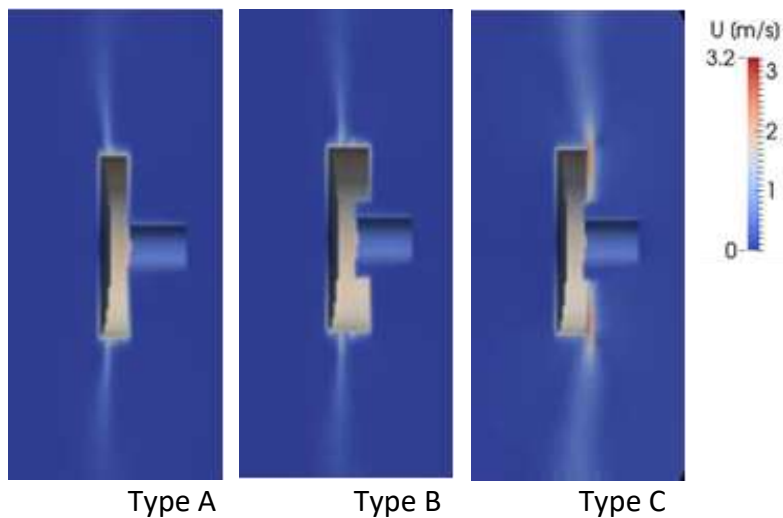
Fig. 5. Distribution of airflow around the ring
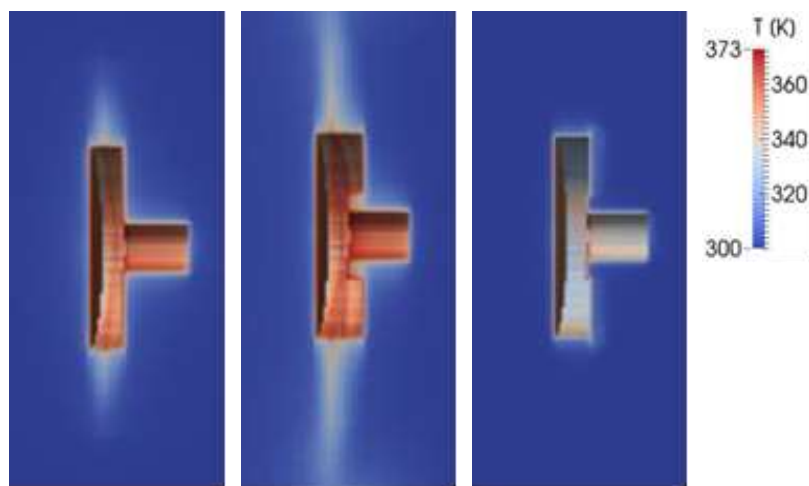
Fig. 6. Distribution of temperature around the ring

Figure 7 shows the time change of the space average heat transfer coefficient for the ring, shaft, and copper plate. As shown in the figure, the spatial average heat transfer coefficient of each component rotates. The value is constant 3 seconds after the start of rotation. From this result, the heat transfer coefficient in each component area is 3 for this simulation. Considering that it becomes a steady value in seconds, the value of the heat transfer coefficient spatially averaged at 3 seconds was used as the boundary condition for heat conduction analysis.
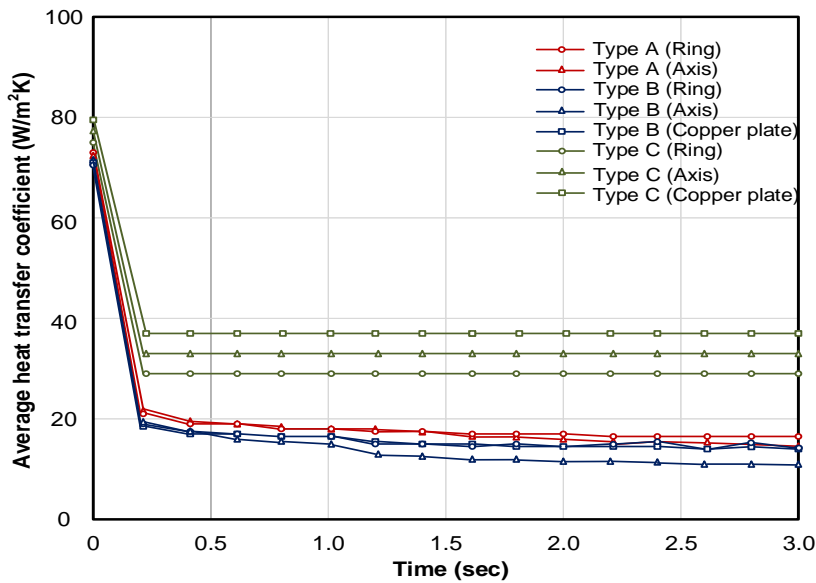
Fig. 7. Time variation of heat transfer coefficient from each part in three-ring types

3.2 Analysis of Heat Conduction Inside the Rotating Body

The spatial average heat transfer coefficient of each region of the ring, shaft, and copper plate obtained by fluid analysis is applied to the surface of each component as a third-class boundary condition. The heat conduction analysis in the composite material was performed. In this study, for the sake of simplicity, the average value and maximum coefficient of friction during the simulation were obtained. Three patterns of heat conduction analysis were performed under each condition with the values and minimum values given as constants. The friction coefficient of each rotating body used in this analysis is shown in Table 2.

Table 2
The friction coefficient was obtained for each ring simulated

Ring Type	Average friction coefficient	Maximum friction coefficient	Minimum friction coefficient
Type A	0.5910	0.9591	0.2573
Type B	0.4334	0.6470	0.2476
Type C	0.5016	0.6679	0.2909

Figure 8 shows a comparison between the simulation results from this study and the experimental results of the time change of the temperature for the ring part when the friction coefficient is taken into consideration. Temperature to evaluate 1 mm from the ring surface where the thermocouple was installed from the experiment. Given the average value of the coefficient of friction, the simulation results were nearly like the experimental results for Type A. Also, the fluctuating experimental results are between the analysis results given the maximum and minimum friction coefficients. Therefore, it is considered that the analysis result of Type A can express the experimental result. For Type B and C, the results show a different trend compared to the experimental results. For the simulation purpose, thermal resistance between the ring test piece and the copper plate in the experimental work was neglected.

Other analyses were the temperature rise of the ring test piece in consideration of thermal resistance. With a ring, the effect of thermal resistance was modelled by assuming that an air layer

was formed between the ring and the copper plate at the sum of the maximum roughness of the copper plate. Figure 9 shows a comparison between the simulation results and the experimental results when the friction coefficient and thermal resistance are taken into consideration. By considering the thermal resistance of Type B and Type C, the analysis results obtained agreed very well with the experimental results. Therefore, it is considered that the experimental results could be reproduced in general, and the constructed analysis model was constructed. It is considered that we were able to show the effectiveness of the system.
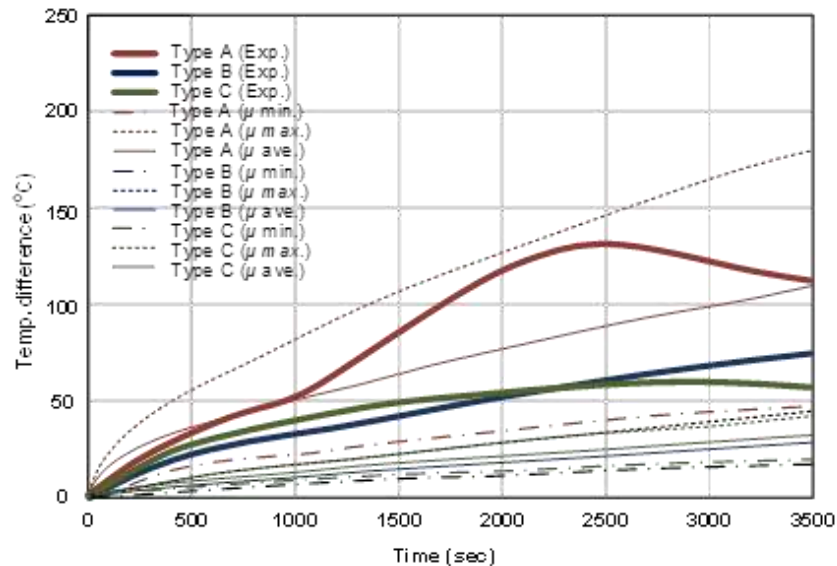
Fig. 8. Simulation and the experimental results of the time change of the temperature for the ring part for case friction coefficient

Summarizing the above results, the following can be considered. In the rotating body for Type A, the heat dissipation mechanism is convection heat transfer from the ring surface. Considering the change in the coefficient of friction from Figure 9, the simulation model shows the temperature change of the rotating body for Type A. It became clear to predict to some extent Type A. This result is the spatial average heat transfer coefficient by the centralized heat capacity model assumed in this study. It shows the effectiveness of the numerical model used. It also shows the effectiveness of modelling the frictional heat effect given as an isobaric boundary condition. It is probable that by considering thermal resistance, the temperature of the rotating body Type B and Type C is composed of composite parts. Since the time variation of the distribution is also matched, it is possible to show the possibility that this analysis model can be used even in a more practical system.
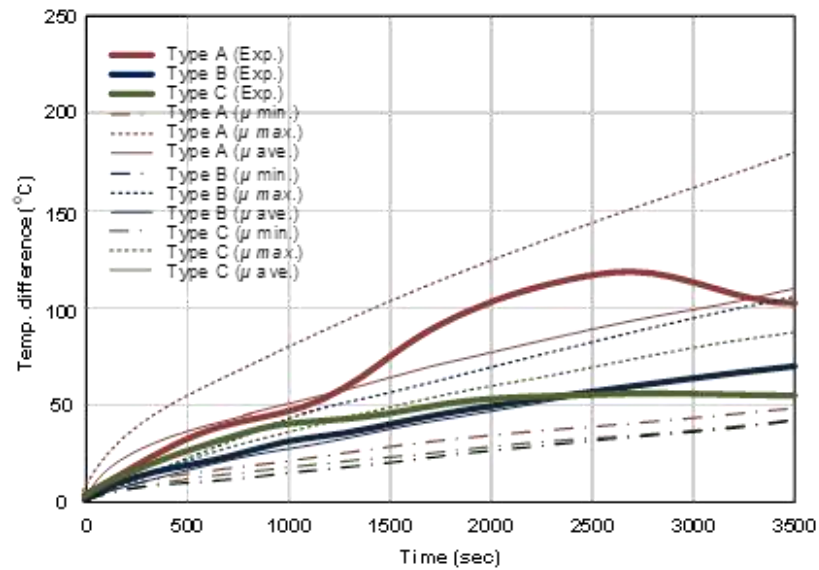
Fig. 9. Simulation and the experimental results when the friction coefficient and thermal resistance are taken into consideration

The effectiveness of this analysis model was shown in fluid analysis and heat conduction analysis, which are extremely expensive to calculate. It is thought that it was possible. It is shown that the phenomenon can be predicted by one-way analysis from fluid analysis to heat conduction analysis without performing direct coupled analysis. Since the numerical investigation for the heat conduction effect can be performed at high-speed simulation only, it is thought that it will be possible to shorten the time for a large amount of simulation during practical calculation using this numerical model.

4. Conclusions

In this research, the authors constructed an analytical modelling of the heat transfer mechanism of a rotating body in a PEEK resin slide bearing using OpenFOAM. To achieve the objectives, a numerical simulation was conducted to measure the temperature distribution of the sliding rotating body when the heat sink was attached. The simulation results were compared with the experimental work and it agree very well with the available experimental data. With the model developed for validation, a simulation of heat conduction in the rotating body when the heat sink is attached was performed and compared with the experimental. From the result obtained, a conclusion was made about the effectiveness of the constructed numerical model. Based on the friction and wear test results, by applying a heat dissipation mechanism to the ring test piece, the calorific value of the PEEK material can be reduced, and it is stable. It was suggested that the friction was maintained. From the experiment.

References

[1] Kurdi, A., Kan, W.H., and Chang, L. "Tribological Behaviour of High-Performance Polymers and Polymer Composites at Elevated Temperature." *Tribology International* 130 (2019): 94–105. https://doi.org/10.1016/j.triboint.2018.09.010

[2] Urmi, W.T., Rahman, M.M., Safiei, W., Kadirgama, K., and Maleque, M.A., "Effects of Minimum Quantity Lubrication Technique in Different Machining Processes - A Comprehensive Review." *Journal of Advanced Research in Fluid Mechanics and Thermal Sciences* 90. No. 2 (2022), 135–159. https://doi.org/10.37934/arfmts.90.2.135159

[3] Chang, L. Zhang, Z. Ye, L. Friedrich, K. "Tribological Properties of High-Temperature Resistant Polymer Composites with Fine Particles." *Tribology International* 40, no.7 (2007): 1170–78. https://doi.org/10.1016/j.triboint.2006.12.002

[4] Myshkin, N.K., Petrokovets, M.I. and Kovalev, A.V. "Tribology of Polymers: Adhesion, Friction, Wear, and Mass-Transfer." *Tribology International* 38, no. 11-12 (2005): 910–21. https://doi.org/10.1016/j.triboint.2005.07.016

[5] Safiei, W., Rahman, M.M., Yusoff, A.R., Tasnim, W., and Malek, Z.A.A., "Evaluation of Cutting Force in End Milling Process of Aluminium Alloy 6061-T6 Using Tungsten Carbide Inserts with MQL Method Utilizing Hybrid Nanofluid." *Journal of Advanced Research in Fluid Mechanics and Thermal Sciences* 84, no. 1 (2021): 111-125. https://doi.org/10.37934/arfmts.84.1.111125

[6] Rasep, Z, Muhammad Yazid, M.N.A.W., Samion, S., & Sidik, N.A.C., "Potential of RBD Palm Oil as a Lubricant in Textured Journal Bearing using CFD with Consideration of Cavitation and Conjugate Heat Transfer." *CFD Letters*, 14, no.2 (2022): 98–110. https://doi.org/10.37934/cfdl.14.2.98110

[7] Xiao, S. and Sue, H.-J. "Effect of Molecular Weight on Scratch and Abrasive Wear Behaviors of Thermoplastic Polyurethane Elastomers." *Polymer* 169 (2019): 124–30 https://doi.org/10.1016/j.polymer.2019.02.059

[8] Quan, D., Deegan, B., and Binsfeld, L. "Effect of Interlaying UV-Irradiated PEEK Fibres on the Mechanical, Impact and Fracture Response of Aerospace-Grade Carbon Fibre/Epoxy Composites." *Composites Part B: Engineering* 191 (2020): 107923. https://doi.org/10.1016/j.compositesb.2020.107923

[9] Akagaki, T., Kuraoka, Y., Takeo, F., Furuya, K. and Kawabata, M. "Effects of PEEK's Surface Roughness on Seizure Behaviors of PEEK/Steel Pairs under Oil-Lubricated Sliding Contacts." *Mechanical Engineering Journal* 4, no. 5 (2017): 17-0001517-00015. https://doi.org/10.1299/mej.17-00015

[10] Akagaki, T., Nakamura, T. Hashimoto, Y and Kawabata, M. "Effects of Material Combinations on Friction and Wear of PEEK/Steel Pairs under Oil-Lubricated Sliding Contacts." *Journal of Physics: Conference Series,* 843, (2017): 012071. http://dx.doi.org/10.1088/1742-6596/843/1/012071

[11] Mir, A.H. and Charoo M.S. "Friction and Wear Characteristics of Polyetheretherketone (PEEK): A Review." *IOP Conference Series: Materials Science and Engineering* 561, no. 1 (2019): 012051. DOI:10.1088/1757-899X/561/1/012051

[12] Tian, Renjie, Guangming Zhu, Yuwei Lv, Taotao Wu, Tianning Ren, Zhiliang Ma, and Shuang Zhang. "Experimental Study and Numerical Simulation for the Interaction between Laser and PEEK with Different Crystallinity." *High Performance Polymers* 33, no. 8 (2021): 851–61. https://doi.org/10.1177/0954008321996771

[13] Zaman, I., Khalid, A., Manshoor, B., Araby, S., Ghazali, M.I. "The Effects of Bolted Joints on Dynamic Response of Structures." *IOP Conference Series: Materials Science and Engineering* 50, no. 1 (2013): 012018. http://dx.doi.org/10.1088/1757-899X/50/1/012018

[14] Akagaki, T., and Kawabata, M. "Effects of Counterface Surface Roughness on Friction and Wear of PEEK Materials under Oil-Lubricated Conditions." *Tribology Online* 11, no. 3 (2016): 494–502. DOI:10.2474/trol.11.494

[15] Akagaki, T., and Kawabata, M. (2010). "Seizure of PEEK and Its Composite at High Sliding Velocity in Oil Lubrication." *In Advance Tribology*, 378–83. Berlin: Springer. https://doi.org/10.1007/978-3-642-03653-8_118

[16] Zhang, G., Wetzel, B., Jim, B. and Oesterle, W. "Impact of Counterface Topography on the Formation Mechanisms of Nanostructured Tribofilm of PEEK Hybrid Nanocomposites." *Tribology International* 83 (2015): 156–65. https://doi.org/10.1016/j.triboint.2014.11.015

[17] Khalid, A., Azman, N., Zakaria, H., Manshoor, B., Zaman, I., Sapit A. and Leman A.M. "Effects of Storage Duration on Biodiesel Properties derived from Waste Cooking Oil." *Applied Mechanics and Materials* 554, (2014) https://doi.org/10.4028/www.scientific.net/AMM.554.494

[18] Wang, Q-H., Xue, Q-J., Liy, W-M. and Chen, J-M. "The Friction and Wear Characteristics of Nanometer SiC and Polytetrafluoroethylene Filled Polyetheretherketone." *Wear* 243, no. 1-2 (2000): 140–46. https://doi.org/10.1016/S0043-1648(00)00432-4

[19] Kovalenko, P., Perepelkina, S. and Korakhanov, T. "Investigation of Tribological Properties of Friction Pairs Duralumin – Fluoropolymer Used for Design and Manufacturing of Biomechatronic Devices." *Tribology in Industry* 39, no. 2 (2017): 192–97. DOI:10.24874/ti.2017.39.02.05

[20] Khalid, A., Mudin, A., Jaat, M., Mustaffa. N., Manshoor, B., Ali, M.F.M., Razali, M.A., Ngali, Z., "Effects of Biodiesel Derived by Waste Cooking Oil on Fuel Consumption and Performance of Diesel Engine." *Applied Mechanics and Materials* 554, (2014): 520-525. DOI:10.4028/www.scientific.net/AMM.554.520

[21] Manshoor, B., Jaat, M., Izzuddin, Z., and Khalid, A. "CFD Analysis of Thin Film Lubricated Journal Bearing." *Procedia Engineering* 68 (2013): 56–62. https://doi.org/10.1016/j.proeng.2013.12.147

[22] Ovaert, T.C., and Cheng, H.S. "Counterface Topographical Effects on the Wear of Polyetheretherketone and a Polyetheretherketone-Carbon Fiber Composite." *Wear* 150 (1991): 275–87. https://doi.org/10.1016/0043-1648(91)90323-MGet rights and content

[23] Robertson, E., Choudhury, V., Bhushan, S. and Walters, D.K. "Validation of OpenFOAM Numerical Methods and Turbulence Models for Incompressible Bluff Body Flows." *Computers & Fluids* 123 (2015): 122–45. https://doi.org/10.1016/j.compfluid.2015.09.010